Soft Matter

PAPER

View Article Online
View Journal | View Issue

Cite this: *Soft Matter*, 2015, 11, 4600

Shape transformations of soft matter governed by bi-axial stresses†

Héloïse Thérien-Aubin,[a] Michael Moshe,[b] Eran Sharon[b] and Eugenia Kumacheva*[acd]

Received 9th March 2015,
Accepted 23rd April 2015

DOI: 10.1039/c5sm00561b

www.rsc.org/softmatter

Rational design of the programmable soft matter requires understanding of the effect of a complex metric on shape transformations of thin non-Euclidean sheets. In the present work, we explored experimentally and using simulations how simultaneous or consecutive application of two orthogonal perturbations to thin patterned stimuli-responsive hydrogel sheets affects their three-dimensional shape transformations. The final shape of the sheet is governed by the metric, but not the order, in which the perturbations are applied to the system, and is determined by the competition of small-scale bidirectional stresses. In addition, a new, unexpected transition from a planar state to an equilibrium helical shape of the hydrogel sheet is observed *via* a mechanism that is yet to be explained.

Introduction

Over the past few years, there has been revived interest in the studies of shape transitions in soft matter.[1–5] Experimental and theoretical research has been motivated by the availability of new stimuli-responsive materials and their patterning methods,[6–10] the desire to understand and mimic the mechanics of biological systems,[4,11–15] and by advances in the development of theoretical models.[16–19]

Planar hydrogel sheets can behave as non-Euclidean plates, thin elastic sheets with a non-flat intrinsic geometry, which do not possess a stress-free configuration.[20–22] The transformation of such sheets from a planar to a three-dimensional (3D) shape stems from residual internal stresses that are programmed in the sheet by inducing stimulus-responsive differential hydrogel swelling.[8,17,23] The selected shape is programmed by prescribing a target metric field on the sheet; this field encodes the equilibrium distances between points on the sheet. The reference metric field can vary on a large scale, that is, a scale comparable with the system size,[15,24–26] or on a small-scale, in which a sharp modulation in swelling and mechanical properties is induced by the pattern with a characteristic feature size significantly smaller than the lateral dimensions of the sheet.[8,27–30] In both cases, even moderate changes in the metric could result in large differences of the final 3D shape of the sheet.

Currently, shape transitions in planar hydrogel sheets patterned with small-scale features are generated by a simple metric.[8,15,27,28,31,32] The lack of understanding of the mechanism of shape transformations of non-Euclidean plates with complex metric limits further advances in the design of self-shaping soft matter. Furthermore, understanding the role of the order, in which multiple stresses are generated in the sheet, is an important step in the design of more elaborate target metrics, which paves the way for producing a programmable soft matter.

Here, we explore the mechanism of shape transitions in thin non-Euclidean polymer sheets under the action of bi-axial stresses. We show how that the competition between the longitudinal and transverse stresses generated by a small-scale metric in a planar hydrogel sheet leads to the shapes with varying unidirectional curvatures and generates a structure with two well-defined and controllable curvatures. In addition, we report a new, unexpected transition between a planar sheet and an equilibrium helical shape. Finally, we show that simultaneous or consecutive generation of longitudinal or transverse stresses does not qualitatively affect shape selection by the non-Euclidean plate, which depends only on its metric. The experimental results are supported by simulations. These findings have impact on the design of environmentally responsive materials in biomechanics, soft robotics, and tissue engineering.

Results and discussion

Fig. 1a illustrates a hydrogel sheet with length L, width w, and thickness t. By using a double-polymerization photolithography method,[27,28] the sheet was patterned with regions of a primary

[a] University of Toronto, Department of Chemistry, 80 Saint George street, Toronto, Ontario, M5S 3H6, Canada. E-mail: ekumache@chem.utoronto.ca
[b] Hebrew University, The Racah Institute of Physic, Jerusalem, Israel
[c] University of Toronto, Department of Chemical Engineering and Applied Chemistry, 200 College Street, Toronto, Ontario, M5S 3E5, Canada
[d] University of Toronto, The Institute of Biomaterials and Biomedical Engineering, 4 Taddle Creek Road, Toronto, Ontario, M5S 3G9, Canada

† Electronic supplementary information (ESI) available: Additional characterization and numerical modelling. See DOI: 10.1039/c5sm00561b

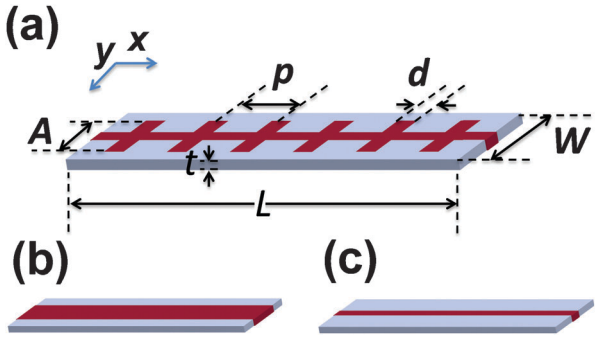

Fig. 1 (a) An illustration of the patterned hydrogel sheets of length L, width w and thickness t. d is the width of the lines of the pattern, A the amplitude of the pattern and p the spacing of the pattern. Red and grey colors correspond to PG and BG regions, respectively. Experimentally used dimensions: w = 1.75 cm, L = 6 cm and 200 $\leq t \leq$ 600 μm. 0.5 $\leq A \leq$ 1.75 cm. $d < p < L$; d = 1 mm. (b) Limiting case 1: $p \leq d$, 0.5 $\leq A \leq$ 1.75 cm. (c) Limiting case 2: $p > L$.

gel (PG) containing one polymer and a binary gel (PG) composed of two polymers. The PG regions (shown with red color) formed a long stripe of width d running parallel to the long x-axis of the sheet and multiple orthogonal stripes of width d and length A, running parallel to the short y-axis of the sheet, and separated from each other with spacing p. Fig. 1b and c show two limiting cases of the PG structure. For $p \leq d$ (case 1), the pattern simplifies to a line of width A (Fig. 1b), while for $p > L$ (case 2), the pattern becomes a single line of width d (Fig. 1c).

In our work, in the first polymer system studied, the PG and BG regions were designed in such a manner that under the application of external stimulus (increased ionic strength of the medium), the PG undergoes strong contraction, while the BG only weakly responds to environmental changes.

The PG and BG regions were formed from poly(*N*-isopropylacrylamide) (pNIPAm) and an interpenetrating network of pNIPAm and poly(2-acrylamido-2-propane sulfonic acid) (pAMPS), respectively. Upon transfer of the hydrogel sheet from deionized water into a 1.5 M solution of NaCl, the regions of PG underwent strong deswelling,[33] while the regions of BG remained highly swollen and pliant, due to the retention of water.[28,34] A strong mismatch in dimensions and mechanical properties between the contracted PG and swollen BG regions created stress at the interface between these domains, and globally, the sheet buckled to reduce these local stresses.

We note that shape transitions in non-Euclidean plates patterned with a contracting stimulus-responsive stripe, as shown in Fig. 1b and c, have been studied.[8,28,30,31] In these studies, when the stripe contracted at elevated temperature or at the increased ionic strength of the surrounding liquid medium, a new metric transformed the sheet into a short roll (a single curvature structure), due to the stresses generated at the interface between the swollen and contracted regions. The more elaborate reference metrics used in the present work led to more diverse configurations. Experimentally, four 3D shapes of the hydrogel sheet were identified (Fig. 2) and mapped on a phase-like diagram plotted in the p–A/w parameter space, where A/w is

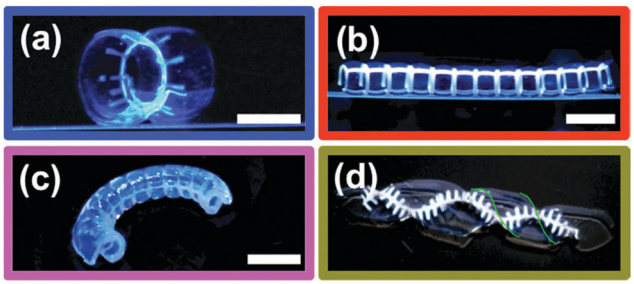

Fig. 2 Photographs of the structures adopted by the hydrogel sheet: (a) a short roll (SR), (b) a long roll (LR), (c) a double curvature (DC) and (d) a helical structure (H). The scale bar is 1 mm. The green lines in (d) outline the front surfaces of the helix and are shown for eye guidance. w = 1.75 cm, L = 6 cm, t = 300 μm, d = 1 mm, 0.5 $\leq A \leq$ 1.75 cm and $d < p < L$.

the length of the transverse PG lines normalized by the width of the sheet (Fig. 3).

Hydrogel sheets exhibited small-scale wavy shape modulations (with a scale set by p), which were superimposed on large-scale 3D configurations. These shapes can be viewed as obtained by coarse graining, that is, by viewing the 3D configuration with a low spatial resolution.

At low and high values of p, in the entire range of the ratios A/w, the effect of PG shrinkage was analogous to the effect of contraction of a single PG stripe running parallel to the x-axis and generating a longitudinal stress in the sheet. To relax this stress, the sheet bent in the longitudinal direction and formed a short roll (SR) (Fig. 2a and regions SR in Fig. 3), in agreement with earlier reports.[28,30,31]

For $d < p < L$ and A/w = 1 (the transverse lines running across the entire sheet width), the transverse stress significantly exceeded the longitudinal one. The sheet formed a long roll (LR) with a single curvature, in a coarse-grained view, along the y-axis (Fig. 2b and region LR in Fig. 3). This shape was also obtained in the absence of the longitudinal stripe, that is, with only the transverse PG lines patterned in the sheet. For A/w = 1 and $p = L$,

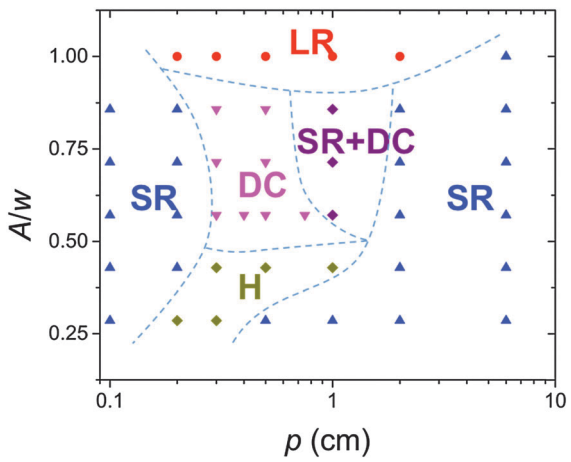

Fig. 3 Phase-like diagram of the generated structures mapped in the p–A/w parameter space. w = 1.75 cm, L = 6 cm, t = 300 μm, d = 1 mm, 0.5 $\leq A \leq$ 1.75 cm and $d < p < L$. The color of symbols corresponds to the color of frames in Fig. 2.

the PG pattern simplified to a longitudinal line and the formation of SR was favored. For the limiting case 1, where $A/w = 1$ and $p < d$, no shape change occurred, as the hydrogel sheet was composed of PG only.

At the intermediate values of p and A/w two other shape transitions took place. A double-curved (DC) structure formed at $0.2 < p < 1$ cm and $0.60 < A/w < 0.85$ (Fig. 2c and region DC in Fig. 3). The curvatures in the longitudinal and transverse directions emerged concomitantly (see ESI†). The formation of the helical structure (H) was observed when transverse lines with a low amplitude were separated by a moderately large spacing p, that is, $0.1 < p < 1$ cm and $0.28 < A/w < 0.57$ (Fig. 2d and region H in Fig. 3).

Fig. 4 shows the effect of the metric of the hydrogel sheet on the coarse-grained curvatures along its transverse and longitudinal axes. The principal curvatures, k_1 and k_2, were determined as the inverse of the measured radii of curvatures, R_1 and R_2 (Fig. 4a). The variation in k_1 and k_2 was studied as a function of spacing p and the normalized amplitude A/w of the transverse perturbations, and thickness t of the sheet.

Fig. 4b shows the effect of spacing p on the curvatures of the hydrogel sheet. In the intermediate range of p, a structure with a double curvature with $k_1 \neq 0$ and $k_2 \neq 0$ formed (region DC between the two vertical dashed lines in Fig. 4b). Double curvature was observed when the stresses created by the polymer actuation in the PG domains along both axes were comparable. This led to the existence of DC structures only in a limited region of the A/w–p space. In this regime, the coarse-grained configuration is doubly curved, thus has a non-zero Gaussian curvature.

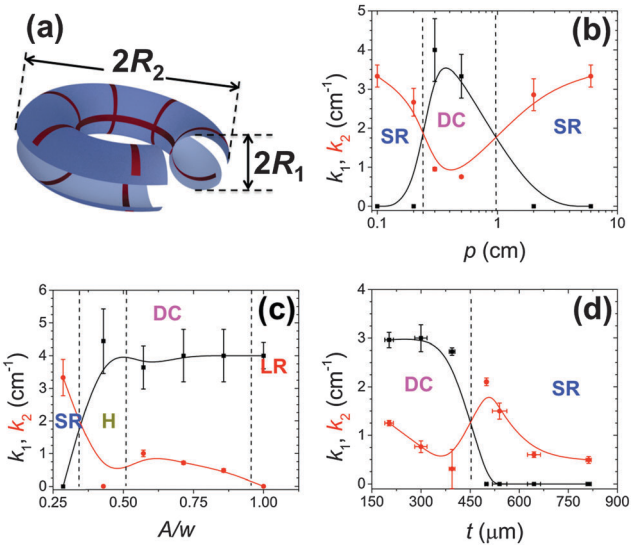

Fig. 4 Effect of the structural characteristics of the hydrogel sheet on its equilibrium curvatures. (a) Schematic of the structure with two radii of curvature, R_1 and R_2, (corresponding to the curvatures $k_1 = 1/R_1$ and $k_2 = 1/R_2$, respectively). Dependence of the curvatures of the sheet on (b) the spacing between the transverse PG lines. $A/w = 0.85$, $d = 1$ mm, $t = 300$ μm; (c) the normalized amplitude A/w of PG pattern. $p = 0.5$ cm, $d = 1$ mm, $t = 0.5$ mm; (d) hydrogel sheet thickness. $A/w = 0.85$ cm, $p = 0.5$ cm, $d = 1$ mm. The dashed lines represent the boundaries between the different hydrogel shapes specified in Fig. 2.

Such a geometry requires the distance between transverse lines in Fig. 4a to increase towards the edge, while their reference distance is constant and leads to significant stresses on a large scale. At small and high values of p, the PG pattern approached a thin line of thickness d or a thick line of thickness A (limiting cases 1 and 2 in Fig. 1b and c, respectively), thereby yielding $k_1 = 0$, characteristic of the SR regime.

Fig. 4c shows the relationship between the curvatures of the sheet and the amplitude of the transverse PG lines. At low A/w values, the formation of SR ($k_1 = 0$) was favored. With an increasing ratio of A/w, the value of k_1 increased and then levelled off in the helical (H), double curvature (DC) and long roll (LR) regimes. The longitudinal curvature k_2 exhibited a more complex behavior. For the intermediate A/w values, k_2 strongly increased (DC regime, Fig. 4c), while at high A/w values, the transverse stress dominated and the sheet returned to the LR regime ($k_2 = 0$).

Fig. 4d shows that with an increase in thickness t of the sheet, both k_1 and k_2 of the DC structure decreased, due to the increasing bending rigidity of the sheet, similarly to the observations on strips with unidirectional stripes.[27,28,30] At sufficiently large thickness t, the transverse bending mode reduced below its buckling threshold,[21,27] leading to $k_1 = 0$. Beyond this point the resulting shape was similar to that of a non-Euclidean plate with a single contracted longitudinal PG stripe. Indeed, k_2 increased to a higher equilibrium value, from which it reduced towards it own buckling transition, as observed and calculated.[21,27]

The experimental work was supported by a numerical simulation study. We used finite element modelling to compute the energy minimizing configuration of an elastic sheet with a given reference metric tensor (see ESI†).

Fig. 5 shows the results of simulation of shape transitions in the hydrogel sheet, which produced all the configurations (short rolls (SR), long rolls (LR) and double-curved (DC) sheets) and transitions that were observed experimentally, except for the helical configuration. Moreover, the transitions between these configurations (Fig. 5a and b), qualitatively resembled the experimental phase-like diagram (Fig. 3). These results suggest that the configurations observed experimentally are selected solely by the minimization of the elastic energy in the system.

The origin of the experimentally observed shape transitions can be understood in terms of the competition between the two modes of spontaneous uni-axial buckling. As shown previously,[27] contraction of an array of parallel stimuli-responsive stripes results in sheet bending along the direction of the stripes, which is accompanied by the formation of small-scale waves in the z-direction (perpendicular to the stripes). The coarse grained description of such a sheet is unusual: the striped metric induces only the absolute value of a uni-axial spontaneous curvature. The sheet can buckle up or down with an equal probability, while the coarse grained metric is Euclidean (has a zero Gaussian curvature). In the present work, the bi-directional array of stripes is inconsistent with such Euclidean metric: the two perpendicular uni-directional curvatures k_1 and k_2 can exist only in the presence of a Gaussian curvature.

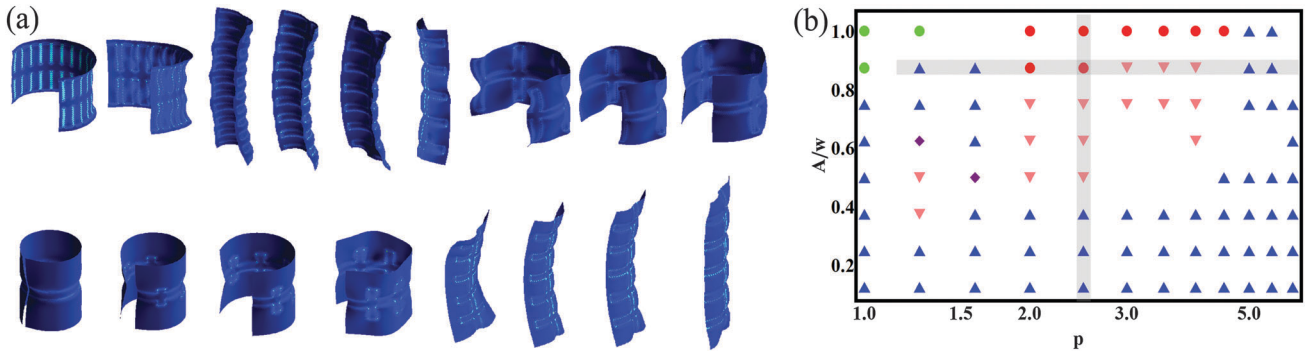

Fig. 5 Three-dimensional structures adopted by the hydrogel sheets obtained by numerical simulations. (a) Selected configurations obtained by numerical minimization of the elastic energy for sheets showing the transition between the short roll regime to the double curvature regime to the short roll regime for sheets with a fixed value of A/w and increasing values of p (top), and showing the transition between the short roll regime to double curvature regime to long roll regime for sheets when p is fixed and the values of A/w increase (bottom). The top panel corresponds to A/w = 7/8, and p of 2, 2.5, 3, 3.5, 4, 4.5, 5, 5.5 and 6 (left to right). The bottom panel corresponds to p = 3.5 and A/w of 1/8, 2/8, 3/8, 4/8, 5/8, 6/8, 7/8 and 1 (left to right). (b) Phase-like diagram of the minimizing configurations for different values of A/w and p. The horizontal and vertical shaded stripes correspond to the top and bottom panels of (a), respectively. Blue triangles: SR, red circles: LR, red triangles: DC, purple diamonds: DC + SR, green circles: sheets with wrinkled edges (not observed experimentally).

The Euclidean nature of the sheet is thus compromised at intermediate values of A/w and p: when these values are comparable a highly stretched sheet acquires a DC shape. Beyond this specific region in the parameter space (Fig. 3), highly energetic DC configurations are replaced with the Euclidean ones. At large values of p and A/w, the effect of shrinkage of the transverse PG stripes is negligible, and the shape is dominated by the contraction of the longitudinal stripe (case 2). The result is a short roll with a varying radius of curvature, as shown previously.[30] The other limiting case (case 1) at $p = d$ yields a similar result.

Next, we designed a polymer system to explore how the sequence of the generation of longitudinal and transverse stresses influences shape transitions in the hydrogel sheet. A rectangular non-responsive poly(acrylamide-*co*-butyl methacrylate) (p(AAM-*co*-BMA)) PG sheet was patterned with two distinct types of temperature-responsive polymers (Fig. 6). The first BG (BG-1) (a red stripe in Fig. 6a) was formed by an interpenetrating network of p(AAM-*co*-BMA) and PNIPAm; the second BG (BG-2) (green stripes in Fig. 6a) was composed of an interpenetrating network of p(AAM-*co*-BMA) and poly(*N*-isopropyl acrylamide-*co*-hydroxyethyl acrylamide) (p(NIPAm-*co*-HEAM)). The lower critical solution temperatures (LCSTs) of BG-1 and BG-2 were 34 ± 2 °C (LCST-1) and 54 ± 2 °C (LCST-2), respectively.

Heating the sheet to a temperature of 40 °C (LCST-1 < 40 °C < LCST-2) led to the selective contraction of the BG-1 stripe, thereby generating a longitudinal stress. The sheet formed a short roll (Fig. 6a.i). Further heating of this roll to T = 70 °C (>LCST-2) generated transverse stress in the sheet, which through the transient shape (Fig. 6a.ii) adopted an equilibrium DC shape (Fig. 6a.iii). The same DC shape formed when the sheet was heated from room temperature directly to T = 70 °C (Fig. 6a.iv) (see ESI†).

In the next step, we patterned the BG-1 and BG-2 regions along the y-axis and x-axis, respectively (the regions shown with red and green colors, respectively, in Fig. 6b). At T = 40 °C, the shrinkage of the BG-1 regions generated the transverse stress transforming the sheet into a long roll (Fig. 6b.i). A transition to a DC shape occurred upon heating this roll to T = 70 °C (Fig. 6b.ii and iii). A similar shape transformation occurred when the sheet was heated directly to 70 °C (Fig. 6b.iv).

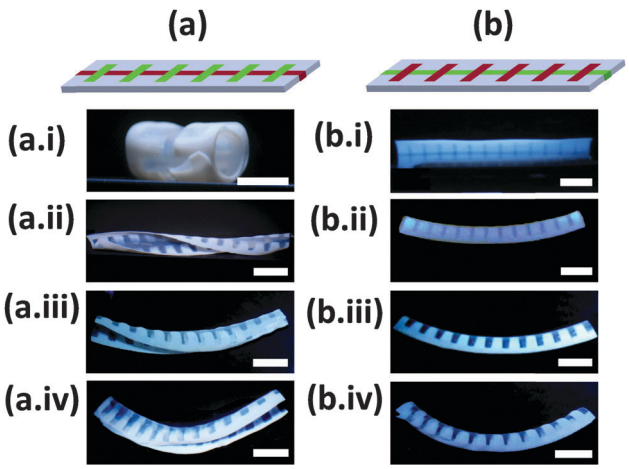

Fig. 6 Effect of the sequence in the generation of longitudinal and transverse stresses on the final hydrogel shape. The contracting BG-1 and BG-2 are shown with red and green colors, respectively. The non-responsive PG is shown with gray color. (a) The sheet is patterned with a longitudinal line of BG-1 and transverse lines of BG-2. (b) The sheet is patterned with a longitudinal line of BG-2 and transverse lines of BG-1. (i) The sheet after 8 h incubation at 40 °C, starting from 25 °C. (ii) The sheet in (i) is incubated for 2 h at 70 °C, starting from 40 °C. (iii) The sheet in (i) is incubated for 12 h at 70 °C, starting from 25 °C. (iv) Gels were incubated overnight at 70 °C from 25 °C. A/w = 0.85, d = 2 mm, t = 250 μm, p = 0.5 cm.

Thus we conclude that for the hydrogel metric used in the present work, the equilibrium shape of the non-Euclidean sheet was independent of the sequence, in which local stresses were generated, and was determined only under the final ambient conditions, although the experimental results cannot be used to rule out the coexistence of two equivalent metastable states. The ultimate shapes shown in Fig. 6a.iii and b.iii evolved through the transient states, in which the original unidirectional curvature of

the hydrogel sheet was compromised, leading to the evolution of the double curved shape.

Conclusions

In summary, we have shown that under the application of external stimuli, small-scale bi-axial residual stresses generated in thin elastic hydrogel sheets (non-Euclidean plates) result in complex 3D shape transformations. Experimental results and simulations show that the competition of metric-dependent longitudinal and transverse stresses is the mechanism of the formation of structures with a well-defined single or double curvature.

Single curvature structures form when either the transverse, or longitudinal stresses dominate, while the formation of a double-curvature configuration occurs in the regime, where both the stresses along the longitudinal and transverse directions are significant. An unexpected helical shape is experimentally observed at a particular metric *via* a mechanism that needs further investigation. Furthermore, we show that the order, in which the longitudinal and transverse stresses are generated, influences the transient structures of the sheet but does not affect its equilibrium shape. These findings have important implications for the design of programmable soft matter materials self-shaping into complex three-dimensional structures.

Experimental section

Materials

All chemicals were purchased from Sigma-Aldrich, unless specified. *N*-Isopropylacrylamide (NIPAM), *N*,*N*′-methylene-bis-acrylamide (MBA), 2-acrylamido-2-propane sulfonic acid (AMPS), acrylamide (AA), and 2-2-azo-bis(2-methylpropionamidine)dihydrochloride (V-50) (Acros) were recrystallized before use. Butyl methacrylate (BMA) and *N*-hydroxyethylacrylamide (HEAM) were purified by column filtration over aluminum oxide.

Synthesis of poly(*N*-isopropyl acrylamide) primary gel (p(NIPAM) PG)

The p(NIPAM) primary gel (PG) sheet was photopolymerized from the aqueous monomer solution containing 14 wt% NIPAm, 1 wt% MBA and 1 wt% V-50, which was placed between two glass plates ($6'' \times 3''$) separated with a silicone rubber spacer with a particular thickness. The reaction cell was then exposed to UV-irradiation (Hönle UVA print 9 mW cm^{-2}) for 25 s. Following this step, $3'' \times 2''$ sheets were cut from the PG base sheet, which were washed in 750 mL of deionized water (changed every 8 h) for 24 h.

Synthesis of p(NIPAM)/poly(2-acrylamido-2-propane sulfonic acid) patterned binary gel (p(NIPAM)/p(AMPS) BG)

The p(NIPAM) sheets were then swollen for 18 h in 250 mL of aqueous monomer solution containing 20 wt% AMPS, 0.25 wt% MBA and 0.5 wt% V-50. The swollen gel was introduced into a reaction cell and exposed to UV-irradiation through a photomask printed on a transparency for 30 s. The interpenetrating network (IPN) was formed in the light-exposed regions of the swollen gel, thereby forming the features of the binary gel (BG). The gel sheets were washed in 750 mL of deionized water (changed every 8 h) for 24 h to remove unreacted reagents and linear, non-crosslinked polymers.

Synthesis of poly(acrylamide-*co*-butyl acrylate) primary gel (p(AA-*co*-BMA) PG)

The p(AA-*co*-BMA) primary gel (PG) sheets were prepared by the photopolymerization of a solution containing 15 wt% of monomer mixture (60 mol% of AA and 40 mol% of BMA), 5 wt% of MBA and 1 wt% of V-50 in a water–DMF mixture (40/60 v%). The reaction cell was exposed for 45 s. The gel sheets were cut in $3'' \times 2''$ sheets and washed for 24 h in 750 mL of water–DMF mixture, which was changed every 8 h, to remove any traces of unreacted monomers.

Synthesis of p(AA-*co*-BMA)/poly(*N*-isopropylacrylamide-*co*-*N*-hydroxyethylacrylamide) patterned binary gel (p(AA-*co*-BMA)/p(NIPAM-*co*-HEAM) BG)

The p(AA-*co*-BMA) PG sheets were swollen for 18 h in 250 mL of aqueous solution of 1 wt% of MBA, 1 wt% of V-50 and 15 wt% of monomer (either 100 mol% NIPAM or of a mixture composed 75 mol% of NIPAM and 25 mol% of HEAM). The swollen gel was introduced into a reaction cell and exposed to UV-irradiation through a photomask printed on a transparency for 45 s. The interpenetrating network (IPN) was formed in the light-exposed regions of the swollen gel, thereby forming the features of the binary gel (BG). The gel sheets were washed in 750 mL of deionized water (changed every 8 h) for 24 h to remove unreacted reagents and linear, non-crosslinked polymers.

Acknowledgements

This work was supported by NSERC Canada (Discovery Grant and Canada Research Chair program). E.S. and M.M. appreciate support of the SoftGrowth project by the European Research Council.

References

1 L. Ionov, *Soft Matter*, 2011, **7**, 6786–6791.
2 D. H. Gracias, *Curr. Opin. Chem. Eng.*, 2013, **2**, 112–119.
3 G. J. Berg, M. K. McBride, C. Wang and C. N. Bowman, *Polymer*, 2014, **55**, 5849–5872.
4 A. R. Studart and R. M. Erb, *Soft Matter*, 2014, **10**, 1284–1294.
5 R. Geryak and V. V. Tsukruk, *Soft Matter*, 2014, **10**, 1246–1263.
6 R. M. Erb, J. S. Sander, R. Grisch and A. R. Studart, *Nat. Commun.*, 2013, **4**, 1712.
7 J. L. Silverberg, A. A. Evans, L. McLeod, R. C. Hayward, T. Hull, C. D. Santangelo and I. Cohen, *Science*, 2014, **345**, 647–650.
8 J. Kim, J. A. Hanna, M. Byun, C. D. Santangelo and R. C. Hayward, *Science*, 2012, **335**, 1201–1205.
9 V. Stroganov, S. Zakharchenko, E. Sperling, A. K. Meyer, O. G. Schmidt and L. Ionov, *Adv. Funct. Mater.*, 2014, **24**, 4357–4363.

10 D. Chen, J. Yoon, D. Chandra, A. J. Crosby and R. C. Hayward, *J. Polym. Sci., Part B: Polym. Phys.*, 2014, **52**, 1441–1461.
11 L. Bertinetti, F. D. Fischer and P. Fratzl, *Phys. Rev. Lett.*, 2013, **111**, 238001.
12 M. J. Harrington, K. Razghandi, F. Ditsch, L. Guiducci, M. Rueggeberg, J. W. C. Dunlop, P. Fratzl, C. Neinhuis and I. Burgert, *Nat. Commun.*, 2011, **2**, 337.
13 S. Armon, O. Yanai, N. Ori and E. Sharon, *J. Exp. Bot.*, 2014, **65**, 2071–2077.
14 S. Armon, E. Efrati, R. Kupferman and E. Sharon, *Science*, 2011, **333**, 1726–1730.
15 Y. Klein, S. Venkataramani and E. Sharon, *Phys. Rev. Lett.*, 2011, **106**, 118303.
16 E. Efrati, E. Sharon and R. Kupferman, *Soft Matter*, 2013, **9**, 8187–8197.
17 E. Sharon and E. Efrati, *Soft Matter*, 2010, **6**, 5693–5704.
18 Z. Y. Wei, Z. V. Guo, L. Dudte, H. Y. Liang and L. Mahadevan, *Phys. Rev. Lett.*, 2013, **110**, 215501.
19 A. Yavari, *J. Nonlinear Sci.*, 2010, **20**, 781–830.
20 J. Gemmer and S. C. Venkataramani, *Soft Matter*, 2013, **9**, 8151–8161.
21 M. Moshe, E. Sharon and R. Kupferman, *Nonlinearity*, 2013, **26**, 3247–3258.
22 Y. Klein, E. Efrati and E. Sharon, *Science*, 2007, **315**, 1116–1120.
23 G. Stoychev, S. Zakharchenko, S. Turcaud, J. W. C. Dunlop and L. Ionov, *ACS Nano*, 2012, **6**, 3925–3934.
24 C. D. Santangelo, *Europhys. Lett.*, 2009, **86**, 34003.
25 B. Audoly and A. Boudaoud, *Phys. Rev. Lett.*, 2003, **91**, 861051.
26 E. Sharon, B. Roman, M. Marder, G. S. Shin and H. L. Swinney, *Nature*, 2002, **419**, 579.
27 Z. L. Wu, M. Moshe, J. Greener, H. Thérien-Aubin, Z. Nie, E. Sharon and E. Kumacheva, *Nat. Commun.*, 2013, **4**, 1586.
28 H. Thérien-Aubin, Z. L. Wu, Z. Nie and E. Kumacheva, *J. Am. Chem. Soc.*, 2013, **135**, 4834–4839.
29 N. P. Bende, R. C. Hayward and C. D. Santangelo, *Soft Matter*, 2014, **10**, 6382–6386.
30 M. Byun, C. D. Santangelo and R. C. Hayward, *Soft Matter*, 2013, **9**, 8264–8273.
31 J. Kim, J. A. Hanna, R. C. Hayward and C. D. Santangelo, *Soft Matter*, 2012, **8**, 2375–2381.
32 J. Bae, J.-H. Na, C. D. Santangelo and R. C. Hayward, *Polymer*, 2014, **55**, 5908–5914.
33 T. G. Park and A. S. Hoffman, *Macromolecules*, 1993, **26**, 5045–5048.
34 K. Kabiri, M. J. Zohuriaan-Mehr, H. Mirzadeh and M. Kheirabadi, *J. Polym. Res.*, 2010, **17**, 203–212.